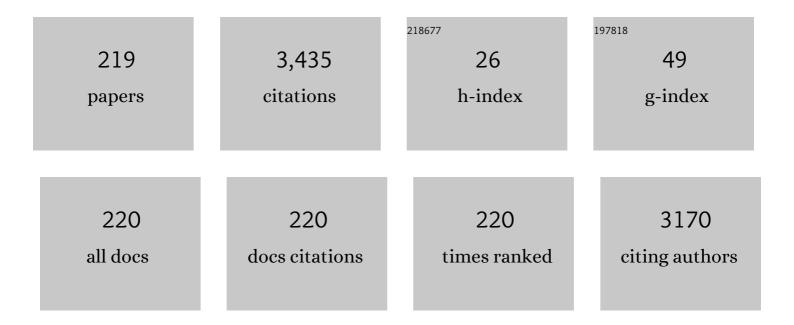
Xue-lin Wang

List of Publications by Year in descending order

Source: https://exaly.com/author-pdf/359167/publications.pdf Version: 2024-02-01



XHE-LIN WANC

#	Article	IF	CITATIONS
1	Excretory-secretory product of Trichinella spiralis inhibits tumor cell growth by regulating the immune response and inducing apoptosis. Acta Tropica, 2022, 225, 106172.	2.0	7
2	β-Glucan-triggered Akkermansia muciniphila expansion facilitates the expulsion of intestinal helminth via TLR2 in mice. Carbohydrate Polymers, 2022, 275, 118719.	10.2	20
3	Extra electric field-enhanced lightning rod effect in pine needle-like Au microarrays for boosting direct plasmon-driven photoelectrochemical hydrogenation reactions via in-situ SERS monitoring. Applied Surface Science, 2022, 578, 152100.	6.1	8
4	Helminth Therapy for Immune-Mediated Inflammatory Diseases: Current and Future Perspectives. Journal of Inflammation Research, 2022, Volume 15, 475-491.	3.5	13
5	Electronic energy loss and ion velocity correlation effects in track production in swift-ion-irradiated LiNbO3: A quantitative assessment between structural damage morphology and energy deposition. Journal of Materials Science and Technology, 2022, 116, 30-40.	10.7	9
6	Effect of Cr and Al on Elastic Constants of FeCrAl Alloys Investigated by Molecular Dynamics Method. Metals, 2022, 12, 558.	2.3	8
7	MoS2/LaF3 for enhanced photothermal therapy performance of poorly-differentiated hepatoma. Colloids and Surfaces B: Biointerfaces, 2022, 214, 112462.	5.0	4
8	Effect of Radiation Defects on Thermo–Mechanical Properties of UO2 Investigated by Molecular Dynamics Method. Metals, 2022, 12, 761.	2.3	1
9	Thermal Spike Responses and Structure Evolutions in Lithium Niobate on Insulator (LNOI) under Swift Ion Irradiation. Crystals, 2022, 12, 943.	2.2	1
10	Organic photovoltaics with 300 nm thick ternary active layers exhibiting 15.6% efficiency. Journal of Materials Chemistry C, 2021, 9, 9892-9898.	5.5	43
11	Comparative multi-omics analyses reveal differential expression of key genes relevant for parasitism between non-encapsulated and encapsulated Trichinella. Communications Biology, 2021, 4, 134.	4.4	4
12	Ag functionalized SnS ₂ with enhanced photothermal activity for safe and efficient wound disinfection. Biomaterials Science, 2021, 9, 4728-4736.	5.4	18
13	Semitransparent organic solar cells exhibiting 13.02% efficiency and 20.2% average visible transmittance. Journal of Materials Chemistry A, 2021, 9, 6797-6804.	10.3	106
14	Ternary Organic Photovoltaic Cells Exhibiting 17.59% Efficiency with Two Compatible Y6 Derivations as Acceptor. Solar Rrl, 2021, 5, 2100007.	5.8	81
15	The immune protection induced by a serine protease from the Trichinella spiralis adult against Trichinella spiralis infection in pigs. PLoS Neglected Tropical Diseases, 2021, 15, e0009408.	3.0	11
16	Over 16% Efficiency of Thickâ€Film Organic Photovoltaics with Symmetric and Asymmetric Nonâ€Fullerene Materials as Alloyed Acceptor. Solar Rrl, 2021, 5, 2100365.	5.8	13
17	Comparative Epigenomics Reveals Host Diversity of the Trichinella Epigenomes and Their Effects on Differential Parasitism. Frontiers in Cell and Developmental Biology, 2021, 9, 681839.	3.7	1
18	Wide Bandgap Polymer with Narrow Photon Harvesting in Visible Light Range Enables Efficient Semitransparent Organic Photovoltaics. Advanced Functional Materials, 2021, 31, 2107934.	14.9	133

#	Article	IF	CITATIONS
19	Alloyed AuPt nanoframes loaded on h-BN nanosheets as an ingenious ultrasensitive near-infrared photoelectrochemical biosensor for accurate monitoring glucose in human tears. Biosensors and Bioelectronics, 2021, 192, 113490.	10.1	19
20	Structural damage response of lanthanum and yttrium aluminate crystals to nuclear collisions and electronic excitation: Threshold assessment of irradiation damage. Journal of Materials Science and Technology, 2021, 90, 95-107.	10.7	6
21	Pronounced interfacial interaction in icosahedral Au@C60 core-shell nanostructure for boosting direct plasmonic photocatalysis under alkaline condition. Journal of Materials Science and Technology, 2021, 94, 10-21.	10.7	5
22	Proteomic Analysis of Taenia solium Cyst Fluid by Shotgun LC-MS/MS. Journal of Parasitology, 2021, 107, 799-809.	0.7	5
23	Investigation on the Correlation between Inclusions and High Temperature Urea Corrosion Behavior in Ferritic Stainless Steel. Metals, 2021, 11, 1823.	2.3	7
24	Label-free serum detection of Trichinella spiralis using surface-enhanced Raman spectroscopy combined with multivariate analysis. Acta Tropica, 2020, 203, 105314.	2.0	7
25	Latent Tracks in Ion-Irradiated LiTaO3 Crystals: Damage Morphology Characterization and Thermal Spike Analysis. Crystals, 2020, 10, 877.	2.2	8
26	Lentinan improved the efficacy of vaccine against Trichinella spiralis in an NLRP3 dependent manner. PLoS Neglected Tropical Diseases, 2020, 14, e0008632.	3.0	13
27	A Low propagation loss planar waveguide structure fabricated on lithium niobate via low fluence argon-ion irradiation. Optik, 2020, 223, 165435.	2.9	0
28	Murine hepatoma treatment with mature dendritic cells stimulated by <i>Trichinella spiralis</i> excretory/secretory products. Parasite, 2020, 27, 47.	2.0	2
29	The immune protection induced by a serine protease from the Trichinella spiralis adult administered as DNA and protein vaccine. Acta Tropica, 2020, 211, 105622.	2.0	11
30	<i>Trichinella spiralis:</i> inflammation modulator. Journal of Helminthology, 2020, 94, e193.	1.0	21
31	Effect of Trichinella spp. or derived antigens on chemically induced inflammatory bowel disease (IBD) in mouse models: A systematic review and meta-analysis. International Immunopharmacology, 2020, 85, 106646.	3.8	4
32	Effects of TLR agonists on immune responses in Trichinella spiralis infected mice. Parasitology Research, 2020, 119, 2505-2510.	1.6	2
33	Effect of recombinant serine protease from newborn larval stage of Trichinella spiralis on 2,4,6-trinitrobenzene sulfonic acid-induced experimental colitis in mice. Acta Tropica, 2020, 211, 105553.	2.0	3
34	Primary characterization of the immune response in pigs infected with Trichinella spiralis. Veterinary Research, 2020, 51, 17.	3.0	28
35	Swift heavy ion tracks in alkali tantalate crystals: a combined experimental and computational study. Journal Physics D: Applied Physics, 2020, 53, 105304.	2.8	12
36	Real-time mass spectrometric characterization of the solid–electrolyte interphase of a lithium-ion battery. Nature Nanotechnology, 2020, 15, 224-230.	31.5	280

#	Article	IF	CITATIONS
37	Over 14.5% efficiency and 71.6% fill factor of ternary organic solar cells with 300 nm thick active layers. Energy and Environmental Science, 2020, 13, 958-967.	30.8	198
38	lon tracks formation through synergistic energy processes in strontium titanate under swift heavy ion irradiation: Experimental and theoretical approaches. Materialia, 2019, 7, 100402.	2.7	7
39	Strontium titanate waveguide in visible and near-infrared regions induced by swift heavy Ni-ion irradiation. Nuclear Instruments & Methods in Physics Research B, 2019, 450, 90-94.	1.4	Ο
40	The effects of ion implantation on rhenium and tin dichalcogenide ultrathin films. Surface and Coatings Technology, 2019, 366, 131-137.	4.8	1
41	Latent tracks and novel infrared waveguide formation in lithium tantalate irradiated with swift heavy ions. Journal Physics D: Applied Physics, 2019, 52, 175303.	2.8	5
42	Regulation of host immune cells and cytokine production induced by <i>Trichinella spiralis</i> infection. Parasite, 2019, 26, 74.	2.0	14
43	Acute shock caused by Clonorchis sinensis infection: a case report. BMC Infectious Diseases, 2019, 19, 1014.	2.9	3
44	Pore structure evolution of IG-110 graphite during argon ion irradiation at 600°C. Journal of Materials Science, 2019, 54, 6098-6110.	3.7	9
45	Atomistic Simulation of Interstitial Dislocation Loop Evolution under Applied Stresses in BCC Iron. Physica Status Solidi (A) Applications and Materials Science, 2018, 215, 1700494.	1.8	2
46	Investigation of Ion–Solvent Interactions in Nonaqueous Electrolytes Using in Situ Liquid SIMS. Analytical Chemistry, 2018, 90, 3341-3348.	6.5	41
47	Tuning the electrical transport of type II Weyl semimetal WTe2 nanodevices by Mo doping. Nanotechnology, 2018, 29, 135705.	2.6	13
48	Modification of WS2 nanosheets with controllable layers via oxygen ion irradiation. Applied Surface Science, 2018, 439, 240-245.	6.1	20
49	Effect of Nb on the Performance of 409 Stainless Steel for Automotive Exhaust Systems. Steel Research International, 2018, 89, 1700558.	1.8	6
50	Ce: Lu2SiO5 optical waveguide by carbon ion irradiation with properties of enhanced photoluminescence. Surface and Coatings Technology, 2018, 342, 117-120.	4.8	4
51	Thermal spike response and irradiation-damage evolution of a defective YAIO3 crystal to electronic excitation. Journal of Nuclear Materials, 2018, 499, 312-316.	2.7	12
52	Reprint of "Ce: Lu2SiO5 optical waveguide by carbon ion irradiation with properties of enhanced photoluminescence". Surface and Coatings Technology, 2018, 355, 273-277.	4.8	0
53	Trichinella spiralis and Tumors: Cause, Coincidence or Treatment?. Anti-Cancer Agents in Medicinal Chemistry, 2018, 18, 1091-1099.	1.7	18
54	Characterization of an antigenic serine protease in the Trichinella spiralis adult. Experimental Parasitology, 2018, 195, 8-18.	1.2	12

#	Article	IF	CITATIONS
55	Cerium-doped lutetium oxyorthosilicate optical waveguide fabricated by ions irradiation: Modification of surface structures and optical properties. Nuclear Instruments & Methods in Physics Research B, 2018, 435, 302-305.	1.4	0
56	The effect of carbon-ion irradiation on surface microstructure and photoluminescence properties in monolayer tungsten diselenide. Nuclear Instruments & Methods in Physics Research B, 2018, 435, 278-284.	1.4	3
57	Microstructural, mechanical and optical properties research of a carbon ion-irradiated Y2SiO5 crystal. Nuclear Instruments & Methods in Physics Research B, 2017, 406, 618-623.	1.4	0
58	lon beam damage assessment and waveguide formation induced by energetic Si-ion irradiation in lanthanum aluminate crystal. Optical Materials, 2017, 64, 391-400.	3.6	11
59	Damage assessment and waveguide fabrication of C ion irradiation on (La, Sr) (Al, Ta)3 crystals. Nuclear Instruments & Methods in Physics Research B, 2017, 406, 566-570.	1.4	0
60	Lattice damage and waveguide properties of medium- and high-energy C3+ ions-irradiated LaAlO3 crystals. Applied Physics B: Lasers and Optics, 2017, 123, 1.	2.2	5
61	Damage evolution and waveguide formation in SrTiO3 crystal irradiated by tens of MeV Si ions. Nuclear Instruments & Methods in Physics Research B, 2017, 406, 606-610.	1.4	2
62	Lattice damage assessment and optical waveguide properties in LaAlO ₃ single crystal irradiated with swift Si ions. Journal Physics D: Applied Physics, 2017, 50, 055303.	2.8	11
63	Coupled electronic and atomic effects on defect evolution in silicon carbide under ion irradiation. Current Opinion in Solid State and Materials Science, 2017, 21, 285-298.	11.5	57
64	An investigation of the beam damage effect on <i>in situ</i> liquid secondary ion mass spectrometry analysis. Rapid Communications in Mass Spectrometry, 2017, 31, 2035-2042.	1.5	13
65	The effects on γ -LiAlO 2 induced by nuclear energy losses during Ga ions implantation. Nuclear Instruments & Methods in Physics Research B, 2017, 406, 624-627.	1.4	1
66	The Raman effects in Î ³ -LiAlO2 induced by low-energy Ga ion implantation. Nuclear Instruments & Methods in Physics Research B, 2017, 409, 72-75.	1.4	6
67	Planar Waveguides in Î ³ -LiAlO2 With Ion Implantation: Light Being Facilely Propagated. Journal of Lightwave Technology, 2017, 35, 19-26.	4.6	6
68	The Lattice Structure and Optical Properties of Neodymium-Doped Gadolinium Vanadate Crystals Induced by Ion Irradiation. IEEE Photonics Journal, 2017, 9, 1-10.	2.0	6
69	Laser-induced convenient synthesis of porous Cu_2O@CuO nanocomposites with excellent adsorption of methyl blue solution. Optical Materials Express, 2017, 7, 924.	3.0	9
70	Laser-induced photochemical synthesis of fibrous-shaped CuO@CuS nanoporous structures for enhanced electrostatic adsorption of negatively charged contaminants from wastewater. Optical Materials Express, 2017, 7, 3863.	3.0	7
71	Immune Cell Responses and Cytokine Profile in Intestines of Mice Infected with Trichinella spiralis. Frontiers in Microbiology, 2017, 8, 2069.	3.5	40
72	Immunoproteomic analysis of the excretory-secretory products of Trichinella pseudospiralis adult worms and newborn larvae. Parasites and Vectors, 2017, 10, 579.	2.5	26

#	Article	IF	CITATIONS
73	Nanoscale imaging of Li and B in nuclear waste glass, a comparison of ToF-SIMS, NanoSIMS, and APT. Surface and Interface Analysis, 2016, 48, 1392-1401.	1.8	14
74	Improving the Molecular Ion Signal Intensity for In Situ Liquid SIMS Analysis. Journal of the American Society for Mass Spectrometry, 2016, 27, 2006-2013.	2.8	46
75	Effects of thermal treatment on structure, surface microstructure and optical properties of nitrogen-ion irradiated nanoparticle thin films. Surface and Coatings Technology, 2016, 306, 87-91.	4.8	0
76	A coupled effect of nuclear and electronic energy loss on ion irradiation damage in lithium niobate. Acta Materialia, 2016, 105, 429-437.	7.9	43
77	Structure and band gap determination of irradiation-induced amorphous nano-channels in LiNbO3. Journal of Applied Physics, 2015, 117, .	2.5	26
78	Fabrication and photoluminescence of strong phase-separated InGaN based nanopillar LEDs. Superlattices and Microstructures, 2015, 88, 323-329.	3.1	19
79	Optical waveguide properties of Ca0.4Ba0.6Nb2O6 crystal formed by oxygen ion irradiation. Nuclear Instruments & Methods in Physics Research B, 2015, 354, 187-191.	1.4	2
80	Optical transmission properties of a planar waveguide structure fabricated on Nd:Li6Y(BO3)3 by C ion irradiation. Nuclear Instruments & Methods in Physics Research B, 2015, 365, 100-104.	1.4	2
81	Two waveguide layers in lithium niobate crystal formed by swift heavy Kr ion irradiation. Chinese Physics B, 2015, 24, 056102.	1.4	3
82	Low Propagation Loss of Single-Mode Planar Waveguides on MgF <inline-formula><tex-math>\$_{f 2}\$ </tex-math></inline-formula> Crystals. Journal of Lightwave Technology, 2015, 33, 2228-2232.	4.6	3
83	Optical planar waveguide in magnesium aluminate spinel crystal using oxygen ion implantation. Applied Physics B: Lasers and Optics, 2015, 120, 25-29.	2.2	2
84	Raman and morphology visualization in epitaxial graphene on 4H-SiC by Nitrogen or Argon ion irradiation. Nuclear Instruments & Methods in Physics Research B, 2015, 365, 260-263.	1.4	6
85	Near-infrared waveguide formation and RBS/channeling spectrometry analysis for damage in calcium barium niobate crystals via ion implantation. Applied Physics B: Lasers and Optics, 2015, 121, 135-139.	2.2	1
86	Magnesium aluminate planar waveguides fabricated by C-ion implantation with different energies and fluences. Nuclear Instruments & Methods in Physics Research B, 2015, 362, 62-67.	1.4	3
87	In Situ Mass Spectrometric Determination of Molecular Structural Evolution at the Solid Electrolyte Interphase in Lithium-Ion Batteries. Nano Letters, 2015, 15, 6170-6176.	9.1	73
88	Escherichia coli and Candida albicans Induced Macrophage Extracellular Trap-Like Structures with Limited Microbicidal Activity. PLoS ONE, 2014, 9, e90042.	2.5	88
89	Visible and near-infrared optical properties of a proton-implanted KTP waveguide. Applied Optics, 2014, 53, 4779.	1.8	2
90	Characterisation of a Plancitoxin-1-Like DNase II Gene in Trichinella spiralis. PLoS Neglected Tropical Diseases, 2014, 8, e3097.	3.0	23

#	Article	IF	CITATIONS
91	Comparison of waveguide properties and Raman spectroscopic visualization of C and O ion implantation on LaAlO_3 crystals. Applied Optics, 2014, 53, 7619.	2.1	4
92	Waveguide and Raman spectroscopic visualization in C-implanted Ca_020Ba_080Nb_20_6 crystal. Optical Materials Express, 2014, 4, 864.	3.0	10
93	Investigation of a chalcohalide glass optical waveguide structure fabricated by dual-energy carbon-ion implantation. Applied Optics, 2014, 53, 278.	1.8	1
94	Nonlinear luminescence response of CaF2:Eu and YAlO3:Ce to single-ion excitation. Journal of Applied Physics, 2014, 115, 033108.	2.5	6
95	Planar and Channel Waveguide Structures in CdS Crystals at 633 and 1539 nm. Journal of Lightwave Technology, 2014, 32, 2556-2559.	4.6	1
96	Ridge waveguide fabrication by combining ion implantation and precise dicing on a LiNbO3 crystal. Nuclear Instruments & Methods in Physics Research B, 2014, 326, 110-112.	1.4	8
97	Optical planar waveguide in sodium-doped calcium barium niobate crystals by carbon ion implantation. Nuclear Instruments & Methods in Physics Research B, 2013, 307, 452-455.	1.4	4
98	Planar waveguide in beta barium borate formed by proton implantation and optical properties in visible and near-infrared band. Optical Materials, 2013, 35, 2068-2071.	3.6	3
99	The near-infrared waveguide properties of an LGS crystal formed by swift Kr8+ ion irradiation. Nuclear Instruments & Methods in Physics Research B, 2013, 315, 328-331.	1.4	5
100	Visible and near-infrared optical properties of chalcogenide glass waveguides formed by swift Kr ion irradiation. Nuclear Instruments & Methods in Physics Research B, 2013, 314, 166-169.	1.4	3
101	Visible and near-infrared waveguides in a chalcogenide glass via dual-energy ion implantation. Optical Materials, 2013, 36, 376-379.	3.6	1
102	Planar and channel waveguides in fused silica fabricated by multi-energy C ion in the visible and near-infrared band. Nuclear Instruments & Methods in Physics Research B, 2013, 307, 472-476.	1.4	5
103	Optical properties of planar waveguide in Nd:YVO4 crystal formed by swift Kr8+ ion irradiation. Nuclear Instruments & Methods in Physics Research B, 2013, 307, 459-462.	1.4	1
104	Planar waveguide structure formed on Nd:YVO4 by Kr8+ ion irradiation at ultralow fluences. Nuclear Instruments & Methods in Physics Research B, 2013, 315, 321-324.	1.4	1
105	Effect of austenite grain size and accelerated cooling start temperature on the transformation behaviors of multi-phase steel. Science China Technological Sciences, 2013, 56, 66-70.	4.0	11
106	Response properties of YAlO3:Ce scintillation crystal under ion irradiation. Nuclear Instruments & Methods in Physics Research B, 2013, 307, 49-54.	1.4	3
107	Visible and near-infrared planar waveguide structure of polycrystalline zinc sulfide from C ions implantation. Optics Express, 2013, 21, 4671.	3.4	14
108	Thermal annealing property of KOTiPO_4 planar and ridge waveguides formed by MeV Si ion implantation. Optical Materials Express, 2013, 3, 426.	3.0	13

#	Article	IF	CITATIONS
109	Effects of swift argon-ion irradiation on the proton-exchanged LiNbO ₃ crystal. Chinese Physics B, 2012, 21, 056103.	1.4	4
110	Waveguide structures for the visible and near-infrared wavelength regions in near-stoichiometric lithium niobate formed by swift argon-ion irradiation. Optics Express, 2012, 20, 4213.	3.4	17
111	Low-loss optical waveguides and Y-branch splitters in lithium niobate fabricated by MeV oxygen ions with low dose. Optics Express, 2012, 20, 21114.	3.4	16
112	Nd:Li6Y(BO3)3 crystal waveguide properties at wavelengths of 633 and 1539 nm produced by oxygen or silicon ion implantation. Applied Optics, 2012, 51, 1681.	1.8	6
113	The Optical and Fluorescence Properties of Planar and Channel Waveguides in Laser Crystal Nd:SrGdGa\$_{3}\$O\$_{7}\$ Formed by Carbon Ion Implantation. Journal of Lightwave Technology, 2012, 30, 2163-2167.	4.6	3
114	Visible and near-infrared waveguide properties in LiTaO3 crystal produced by swift Ar8+ ion irradiation. Applied Physics B: Lasers and Optics, 2012, 108, 675-681.	2.2	8
115	Lattice damage and waveguide properties of a proton-exchanged LiNbO3 crystal after oxygen-ion implantation. Nuclear Instruments & Methods in Physics Research B, 2012, 286, 318-321.	1.4	1
116	Planar and channel waveguides on Na:CBN formed by oxygen ion implantation. Nuclear Instruments & Methods in Physics Research B, 2012, 286, 322-325.	1.4	2
117	Oral immunisation of mice with a recombinant rabies virus vaccine incorporating the heat-labile enterotoxin B subunit of Escherichia coli in an attenuated Salmonella strain. Research in Veterinary Science, 2012, 93, 675-681.	1.9	2
118	Second harmonic generation in periodically poled LiNbO ₃ waveguides formed by oxygenâ€ion implantation. Physica Status Solidi - Rapid Research Letters, 2012, 6, 205-207.	2.4	10
119	Annealing behavior of LiNbO3 planar waveguides formed by oxygen ion implantation. Nuclear Instruments & Methods in Physics Research B, 2012, 272, 116-120.	1.4	2
120	Formation of a highly Erbium doped silicon-on-insulator layer by introducing SiOx on or into a silicon surface. Nuclear Instruments & Methods in Physics Research B, 2012, 278, 1-3.	1.4	2
121	The plant alkaloid piperine as a potential inhibitor of ethidium bromide efflux in Mycobacterium smegmatis. Journal of Medical Microbiology, 2011, 60, 223-229.	1.8	48
122	Annealing effect on planar waveguides in LiNbO3 produced by oxygen ion implantation. Applied Surface Science, 2011, 257, 1918-1922.	6.1	1
123	An He-implanted optical planar waveguide in an Nd:YGC laser crystal preserving fluorescence properties. Applied Surface Science, 2011, 257, 7310-7313.	6.1	11
124	Planar optical waveguides in Nd:BSO crystals fabricated by He and C ion implantation. Optical Materials, 2011, 33, 385-388.	3.6	9
125	The properties of ion-implanted LiNbO3 waveguides measured by the RBS and ion beam etching stripping methods. Optical Materials, 2011, 33, 1357-1361.	3.6	2
126	Simulation of the Transmission Characteristics of a Hexagonal Photonic Crystal Slab Etched into an Ion-implanted LiNbO3 Waveguide. Journal of the Korean Physical Society, 2011, 58, 886-889.	0.7	1

#	Article	IF	CITATIONS
127	Simulation of Transmission Behaviors of Photonic Crystal Structures Etched into an Ion-implanted LN Waveguide. , 2011, , .		0
128	The array waveguides formed in LiNbO3 crystal by oxygen-ion implantation. Nuclear Instruments & Methods in Physics Research B, 2010, 268, 2923-2925.	1.4	6
129	The fabrication of planar waveguides on Bi12TiO20 crystals by oxygen and helium ion implantation. Nuclear Instruments & Methods in Physics Research B, 2010, 268, 3434-3437.	1.4	4
130	In vitro synergistic activity between 8-methoxypsoralen and ethambutol, isoniazid, and rifampin when used in combination against Mycobacterium tuberculosis. World Journal of Microbiology and Biotechnology, 2010, 26, 623-628.	3.6	3
131	1×4-Branch waveguide power splitters in lithium niobate by means of multi-energy O ion implantation. Optical Materials, 2010, 32, 1441-1445.	3.6	14
132	Study on preventing segregation of erbium atoms to a silicon surface by annealing in oxygen atmosphere at high temperature. Nuclear Instruments & Methods in Physics Research B, 2010, 268, 1585-1587.	1.4	8
133	In vitro synergistic interactions of oleanolic acid in combination with isoniazid, rifampicin or ethambutol against Mycobacterium tuberculosis. Journal of Medical Microbiology, 2010, 59, 567-572.	1.8	46
134	Investigation of the lateral spread of erbium ions implanted in silicon crystal. Chinese Physics B, 2010, 19, 113403.	1.4	8
135	Refractive index change in ion-implanted LiNbO3 waveguides calculated from lattice damage ratio. Journal of Applied Physics, 2010, 108, 093103.	2.5	9
136	Planar waveguides in Nd:SGG crystal formed by He ion implantation. Applied Optics, 2010, 49, 6039.	2.1	2
137	Optical properties of planar waveguides on ZnWO_4 formed by carbon and helium ion implantation and effects of annealing. Optics Express, 2010, 18, 18989.	3.4	15
138	Lithium Niobate Ridge Waveguides Fabricated by Ion Implantation Followed by Ion Beam Etching. Journal of Lightwave Technology, 2010, 28, 1913-1916.	4.6	15
139	Optical Waveguide Formed in LiTaO3 Crystal by MeV C3+ Ion Implantation. Journal of the Korean Physical Society, 2010, 56, 1364-1368.	0.7	4
140	Morphology characterization and mechanism analysis of LiNbO3 microstructure by focused ion beam milling. Journal of the Korean Physical Society, 2010, 56, 1369-1373.	0.7	1
141	Investigation of etching two-dimensional microhole lattice array on lithium niobate with focused ion beam for fabricating photonic crystals. Journal of Vacuum Science & Technology B, 2009, 27, 1851.	1.3	2
142	Antifungal activity of thymol against clinical isolates of fluconazole-sensitive and -resistant Candida albicans. Journal of Medical Microbiology, 2009, 58, 1074-1079.	1.8	81
143	Property Studies of Optical Waveguide Formed by keV He-Ion Implanted into a Nd:CNGG Crystal. Journal of the Korean Physical Society, 2009, 55, 2638-2641.	0.7	10
144	Characterization of optical waveguides in β-BaB2O4 crystals formed by 3.0-MeV Cu2+-ion implantation. Applied Physics B: Lasers and Optics, 2008, 91, 139-143.	2.2	3

#	Article	IF	CITATIONS
145	Characterization of optical waveguides in β-BaB2O4 crystals formed by 3.0MeV Ni2+ ions implantation. Applied Surface Science, 2008, 254, 5095-5099.	6.1	3
146	Characterization of optical waveguide in Nd: LuVO4 crystals by triple-energy oxygen ion implantation. Physica B: Condensed Matter, 2008, 403, 679-683.	2.7	2
147	Formation of planar waveguide in BiB3O6 crystal by MeV carbon implantation. Nuclear Instruments & Methods in Physics Research B, 2008, 266, 899-903.	1.4	7
148	Characterization of optical waveguides in YbVO_4 crystals formed by 30 MeV oxygen ion implantation. Applied Optics, 2008, 47, 1117.	2.1	2
149	Optical Channel Waveguides in \$hbox {KTiOPO}_{4}\$ Crystal Produced by Proton Implantation. Journal of Lightwave Technology, 2008, 26, 1304-1308.	4.6	13
150	Active waveguide in Nd3+:MgO:LiNbO3 crystal produced by low-dose carbon ion implantation. Applied Physics Letters, 2008, 92, 021110.	3.3	10
151	Formation of reconfigurable optical channel waveguides and beam splitters on top of proton-implanted lithium niobate crystals using spatial dark soliton-like structures. Journal Physics D: Applied Physics, 2008, 41, 102001.	2.8	13
152	Reconstruction of refractive index profiles of 3 MeV O ²⁺ ion-implanted MgO-doped LiNbO ₃ using wet etching and ellipsometry. Journal Physics D: Applied Physics, 2008, 41, 065302.	2.8	2
153	Monomode low loss optical waveguide in KTiOPO4 formed by combining ion implantation with ion exchange. Journal of Applied Physics, 2008, 104, 063115.	2.5	6
154	Diverse mechanism of refractive index modification in neodymium-doped KGd(WO4)2 crystal induced by MeV He+ or C3+ ion implantation for waveguide construction. Journal of Applied Physics, 2008, 103, 083123.	2.5	8
155	The formation of double waveguides in a KTP crystal by combining ion exchange with ion implantation. Journal Physics D: Applied Physics, 2007, 40, 3358-3362.	2.8	4
156	Low-loss planar and stripe waveguides in Nd3+-doped silicate glass produced by oxygen-ion implantation. Journal of Applied Physics, 2007, 101, 053112.	2.5	31
157	Model of refractive-index changes in lithium niobate waveguides fabricated by ion implantation. Physical Review B, 2007, 75, .	3.2	37
158	Optical Properties of KTaxNb1-xO3Waveguides Formed by Carbon and Proton Implantation. Japanese Journal of Applied Physics, 2007, 46, 5885-5888.	1.5	7
159	Optical waveguide in stoichiometric lithium niobate formed by 500 keV proton implantation. Optics Express, 2007, 15, 16880.	3.4	17
160	Selective etching in LiNbO3 combined of MeV O and Si ion implantation with wet-etch technique. Surface and Coatings Technology, 2007, 201, 5081-5084.	4.8	17
161	Ridge optical waveguide in an Er3+/Yb3+co-doped phosphate glass produced by He+ion implantation combined with Ar+ion beam etching. Journal Physics D: Applied Physics, 2007, 40, 6545-6548.	2.8	23
162	Formation of planar optical waveguide by multi energy Si ion implantation into Nd:YVO4 crystal. Surface and Coatings Technology, 2007, 201, 5427-5430.	4.8	11

#	Article	IF	CITATIONS
163	Ion beam etched diffraction gratings in fused quartz and lithium niobate. Surface and Coatings Technology, 2007, 201, 5046-5049.	4.8	4
164	Fabrication of waveguides in Yb:YCOB crystal by MeV oxygen ion implantation. Applied Surface Science, 2007, 253, 7360-7364.	6.1	2
165	Characterization of optical waveguide in Nd: GdVO4 by triple-energy oxygen ion implantation. Applied Surface Science, 2007, 253, 9311-9314.	6.1	7
166	Single-mode optical waveguides fabricated in LiNbO3 by multienergy C2+ implantations. Optics and Laser Technology, 2007, 39, 749-753.	4.6	5
167	Development of ion-implanted optical waveguides in optical materials: A review. Optical Materials, 2007, 29, 1523-1542.	3.6	288
168	Planar waveguides in calcium barium niobate fabricated by MeV He ion implantation. Applied Physics B: Lasers and Optics, 2007, 87, 289-292.	2.2	15
169	Planar optical waveguides formed in \hat{l}^2 -BBO by MeV O+ implantation. Frontiers of Materials Science in China, 2007, 1, 423-426.	0.5	0
170	Characterization of optical planar waveguide in Ce:KNSBN crystal formed by triple-energy helium ion implantation. Applied Surface Science, 2007, 253, 3589-3594.	6.1	4
171	Formation of waveguides in LiNbO3 by 6.0MeV F3+ implantation. Journal of Applied Physics, 2006, 100, 033505.	2.5	4
172	Channel waveguides of LiNbO3 crystals fabricated by low-dose oxygen ion implantation. Journal of Applied Physics, 2006, 100, 056106.	2.5	9
173	Property study of lithium niobate implanted by Nd and O ions. Nuclear Instruments & Methods in Physics Research B, 2006, 246, 364-368.	1.4	0
174	Si2+ ion implanted into stoichiometric lithium niobate crystals: Waveguide characterization and lattice disorder analysis. Nuclear Instruments & Methods in Physics Research B, 2006, 251, 104-108.	1.4	23
175	The optical properties of planar waveguides in LiB3O5 crystals formed by Cu+ implantation. Applied Surface Science, 2006, 253, 2674-2677.	6.1	3
176	Optical channel waveguides in Nd:YVO4 crystal produced by O+ ion implantation. Applied Physics Letters, 2006, 88, 071123.	3.3	38
177	Channel waveguide array in Ce-doped potassium sodium strontium barium niobate crystal fabricated by He+ ion implantation. Applied Physics Letters, 2006, 89, 191102.	3.3	12
178	Planar optical waveguide in potassium titanyl arsenate formed by oxygen ion implantation at low doses. Applied Physics Letters, 2006, 88, 011114.	3.3	11
179	Double waveguide in NdLiP4O12 laser crystal formed by MeV He+ ion implantation. Nuclear Instruments & Methods in Physics Research B, 2005, 227, 271-274.	1.4	3
180	Planar optical waveguide fabricated by silicon ion implantation into AgGaS2 crystal. Nuclear Instruments & Methods in Physics Research B, 2005, 239, 356-360.	1.4	2

#	Article	IF	CITATIONS
181	Pulsed laser deposition of optical waveguide Nd-doped gadolinium vanadate thin films. Journal of Crystal Growth, 2005, 277, 593-598.	1.5	1
182	Structural and optical properties of Nd:LuVO4 waveguides grown on sapphire substrates by pulsed laser deposition. Journal of Crystal Growth, 2005, 277, 269-273.	1.5	1
183	Nd:CdVO4 thin films grown on La3Ga5SiO14 (LGS) and sapphire substrates by pulsed laser deposition properties. Journal of Crystal Growth, 2005, 281, 426-431.	1.5	6
184	Bi-layer optical waveguide formed by double boron ion implantation into strontium barium niobate crystal. Nuclear Instruments & Methods in Physics Research B, 2005, 234, 467-470.	1.4	4
185	Low loss waveguide in Nd3+-doped silicate glass fabricated by carbon ion implantation. Surface and Coatings Technology, 2005, 200, 598-601.	4.8	Ο
186	Influence of oxygen pressure on Nd:LuVO4 films grown by pulsed laser deposition. Materials Research Bulletin, 2005, 40, 1915-1921.	5.2	0
187	Property studies of optical waveguide formed by 6.0 MeV carbon ion implantation into Nd:silicate glass. Journal Physics D: Applied Physics, 2005, 38, 2899-2903.	2.8	4
188	Optical properties of stoichiometric LiNbO3 waveguides formed by low-dose oxygen ion implantation. Applied Physics Letters, 2005, 86, 041103.	3.3	36
189	Property investigation of C+-ion-implanted LiNbO3 planar optical waveguides. Journal of Applied Physics, 2005, 98, 044507.	2.5	15
190	Optical planar waveguide fabricated in Nd:LuVO4 crystal by MeV oxygen implantation. Optics Express, 2005, 13, 675.	3.4	7
191	Investigation and analysis of a single-mode waveguide formed by multienergy-implanted LiNbO3. Optics Express, 2005, 13, 2256.	3.4	12
192	Formation of c-axis oriented ZnO optical waveguides by radio-frequency magnetron sputtering. Optics Express, 2005, 13, 5093.	3.4	45
193	Formation of waveguides by implantation of 3.0MeV Ni2+. Journal of Applied Physics, 2004, 96, 3463-3466.	2.5	12
194	Fabrication of optical waveguides in KTiOAsO4 by He or Si ion implantation. Nuclear Instruments & Methods in Physics Research B, 2004, 215, 389-393.	1.4	11
195	Refractive index profiles of planar optical waveguides in β-BBO produced by silicon ion implantation. Optical Materials, 2004, 27, 459-463.	3.6	10
196	Planar optical waveguides in β-BaB2O4 produced by oxygen ion implantation at low doses. Applied Physics Letters, 2004, 85, 1457-1459.	3.3	39
197	Damage profiles in LiNbO3by low-energy H+implantation. Radiation Effects and Defects in Solids, 2004, 159, 309-314.	1.2	1
198	Monomode optical waveguide excited at 1540 nm in LiNbO3 formed by MeV carbon ion implantation at low doses. Optics Express, 2004, 12, 747.	3.4	24

#	Article	IF	CITATIONS
199	Low propagation loss of the waveguides in fused quartz by oxygen ion implantation. Optics Express, 2004, 12, 4675.	3.4	28
200	Low propagation loss of the waveguides in fused quartz by oxygen ion implantation: errata. Optics Express, 2004, 12, 5285.	3.4	1
201	Depth profiles of MeV heavy ions implanted into Si and lithium triborate. Nuclear Instruments & Methods in Physics Research B, 2004, 225, 503-508.	1.4	3
202	Extraordinary refractive-index increase in MeV B3+ ion-implanted LiNbO3 waveguide. Nuclear Instruments & Methods in Physics Research B, 2003, 211, 346-350.	1.4	18
203	Double optical waveguide in Cu-doped KNSBN crystal formed by MeV boron ion implantation. Applied Surface Science, 2003, 220, 288-292.	6.1	2
204	Analysis of refractive index profile in a silicon ion-implanted KTiOPO4 waveguide. Materials Letters, 2003, 57, 1197-1201.	2.6	4
205	Low-loss optical planar waveguides in YVO4 produced by silicon ion implantation at low doses. Journal of Applied Physics, 2003, 94, 4708-4710.	2.5	24
206	Ion-Implanted Waveguides in a Nd 3+ -Doped Silicate Glass. Chinese Physics Letters, 2003, 20, 1994-1996.	3.3	10
207	Optical waveguides formed in Nd:YVO4 by MeV Si+ implantation. Applied Physics Letters, 2002, 80, 3473-3475.	3.3	49
208	Monomode, nonleaky planar waveguides in a Nd3+-doped silicate glass produced by silicon ion implantation at low doses. Journal of Applied Physics, 2002, 92, 2959-2961.	2.5	12
209	Ion-implanted Nd:YVO_4 planar waveguide: refractive-index characterization and propagation mode reduction. Optics Letters, 2002, 27, 1111.	3.3	18
210	Planar waveguide fabrication and refractive index characterization in Er:NaY(WO4)2 crystal by MeV silicon ion implantation. Materials Letters, 2002, 57, 1021-1024.	2.6	0
211	MeV copper and nickel ion implanted waveguides in Nd:NaY(WO4)2 crystal. Nuclear Instruments & Methods in Physics Research B, 2002, 187, 475-478.	1.4	2
212	Property study on nickel ion implanted planar waveguide in KTiOAsO4 crystal. Nuclear Instruments & Methods in Physics Research B, 2002, 194, 355-358.	1.4	7
213	Property study of Si + -ion-implanted Nd:YVO 4 waveguides. Applied Physics B: Lasers and Optics, 2002, 75, 895-897.	2.2	13
214	Ion-implanted waveguides in Nd3+-doped silicate glass and Er3+/Yb3+ co-doped phosphate glass. Applied Surface Science, 2002, 193, 92-101.	6.1	35
215	MeV Ni+ ion-implanted planar waveguide in Nd:YVO4 crystal. Applied Surface Science, 2002, 199, 307-311.	6.1	12
216	Planar waveguides in Ce:SBN and Cu:KNSBN crystals by 6.0 MeV B3+ ion implantation. Applied Surface Science, 2002, 202, 86-91.	6.1	5

#	Article	IF	CITATIONS
217	Planar waveguides in BiB3O6 and Nd:YVO4 crystals by ion implantation. Applied Surface Science, 2002, 191, 61-66.	6.1	10
218	Lateral spread of Ar+ implanted in SiO2 and Si3 N4 films. Nuclear Instruments & Methods in Physics Research B, 1992, 72, 51-54.	1.4	0
219	Lateral straggling of Hg+ in both amorphized quartz crystal and Ni film by RBS. Physics Letters, Section A: General, Atomic and Solid State Physics, 1990, 150, 277-280.	2.1	3